$^1J_{WSn}$ as a Solution State Predictor for Tungsten−Tin Solid State Bond Length in Sterically Crowded Tungstenocene Stannyl Complexes

T. Andrew Mobley,* Rochelle Gandour, Eric P. Gillis, Kwame Nti-Addae, Rahul Palchaudhuri, Presha Rajbhandari, Neil Tomson, Angel Vargas, and Qi Zheng

Noyce Science Center, Grinnell College, 1116 8th Street, Grinnell, Iowa 50112

Received December 14, 2004

A correlation between the tungsten tin solid state bond distance (r_{WSn}) and the solution state one-bond scalar coupling of tungsten to tin ($^1J_{WSn}$) is reported. This correlation was observed in hydrido- and chlorotungstenocene diorganostannyl chlorides ($Cp_2WXSnClR_2$, X = H (**1**), X = Cl (**2**)) with sterically demanding organic substituents (R = ^{t}Bu (**1a**, **2a**), Ph (**1b**, **2b**)). The different steric demands of the organic substituents (^{t}Bu and Ph) force the complexes **1a** and **1b** (or **2a** and **2b**) to adopt at 190 K in the solid state different, single rotameric conformations. For **1a** and **2a**, the ^{t}Bu substituents occupy the equatorial wedge of the tungstenocene, whereas for **1b** and **2b** the Ph substituents are rotated to place the chlorine in the equatorial wedge. Variable-temperature multinuclear NMR and density functional theory calculations at the B3LYP/LANL2DZ level indicate the possibility of low-lying conformational isomers for complexes **1b**.

Introduction

Mid-transition metal stannyl complexes represent an area of increasing interest[1−9] due to their potential as unique reagents and catalysts. Substantial work[8,9] has already been accomplished in the synthesis and structural characterization of this class of compounds including examples from groups 5, 6, 7, and 8. Of particular interest to us, work in the late 1980s through the mid 1990s by the groups of Lappert,[10,11] Green,[3] Bulychev,[12,13] and Schubert[2,14] established a facile synthetic route for group 6 stannyl complexes and explored the solid and solution state structures of stannyl complexes with both small (Me) and more sterically hindered (*t*-Bu, $CH(SiMe_3)_2$) organic substituents. In the process of exploring the reactive chemistry of transition metal stannyl complexes we synthesized novel members with substituents of different steric and electronic demands and have discovered a divergence in their conformational behavior in both the solid and solution states.

Previous work by Bulychev[13] on complexes of the type $Cp_2MoHSnCl_xMe_{3-x}$ established a structural model in which the tin has small organic substituents. The Mo−Sn bond is affected greatly by the electrophilicity of the tin center, resulting in a shortening of the Mo−Sn bond with increasing electrophilicity. In an elegant argument based upon the tin isomeric shift determined through Mössbauer spectroscopy and scalar coupling between NMR active Sn isotopes and ^{1}H nuclei of the methyl substituents ($^2J_{SnH}$), Bulychev proposed that this shortening was due primarily to a change from hybrid sp^3 to atomic $s + p^3$ orbitals upon successive substitutions of Cl for CH_3 at the tin center. This hybridization change produces a Mo−Sn bond with greater s-character, thereby resulting in (1) a shortening of the Mo−Sn bond, (2) a greater Mössbauer isomeric shift of the tin, and (3) a decrease in the $^2J_{SnH}$ coupling constant due to Sn−CH_3 bonds with greater tin p-character. This explanation was preferred to an alternative in which backbonding from the molybdenum into unoccupied orbitals on the tin center shortens the Mo−Sn bond.

An additional parameter that should be quite sensitive to hybridization changes, the one-bond tungsten tin scalar coupling constant ($^1J_{WSn}$), has surprisingly received little attention in the literature. The current study establishes this easily obtained solution state

* To whom correspondence should be addressed. E-mail: mobleyt@grinnell.edu.

(1) Seebald, S.; Mayer, B.; Schubert, U. *J. Organomet. Chem.* **1993**, *462*, 225−234.
(2) Seebald, S.; Kickelbick, G.; Moeller, F.; Schubert, U. *Chem. Ber.* **1996**, *129*, 1131−1142.
(3) Green, M. L. H.; Hughes, A. K. *J. Organomet. Chem.* **1996**, *506*, 221−227.
(4) Braune, S.; Kazmaier, U. *Angew. Chem., Int. Ed.* **2003**, *42*, 306−308.
(5) Belsky, V. K.; Protsky, A. N.; Molodnitskaya, I. V.; Bulychev, B. M.; Soloveichik, G. L. *J. Organomet. Chem.* **1985**, *293*, 69−74.
(6) Arkhireeva, T. M.; Bulychev, B. M.; Protsky, A. N.; Soloveichik, G. L.; Bel'sky, V. K. *J. Organomet. Chem.* **1986**, *317*, 33−40.
(7) Braune, S.; Pohlman, M.; Kazmaier, U. *J. Org. Chem.* **2004**, *69*, 468−474.
(8) Esteruelas, M. A.; Lledos, A.; Olivan, M.; Onate, E.; Tajada, M. A.; Ujaque, G. *Organometallics* **2003**, *22*, 3753−3765.
(9) Eguillor, B.; Esteruelas, M. A.; Olivan, M.; Onate, E. *Organometallics* **2004**, *23*, 6015−6024.
(10) Harris, D. H.; Keppie, S. A.; Lappert, M. F. *J. Chem. Soc., Dalton Trans.* **1973**, 1653−1658.
(11) Bohra, R.; Hitchcock, P. B.; Lappert, M. F.; Leung, W. P. *Polyhedron* **1989**, *8*, 1884.
(12) Protsky, A. N.; Bulychev, B. M.; Soloveichik, G. L. *Inorg. Chim. Acta* **1983**, *71*, 35−39.
(13) Protsky, A. N.; Bulychev, B. M.; Soloveichik, G. L.; Belsky, V. K. *Inor. Chim. Acta* **1986**, *115*, 121−128.
(14) Seebald, S.; Mayer, B.; Schubert, U. *Inorg. Chem.* **1995**, *34*, 5285−5288.

10.1021/om049006d CCC: $30.25
Publication on Web 07/01/2005

Table 1. Multinuclear NMR Data[a] for Complexes 1a,b and 2a,b

	1a	1b	2a	2b
^{119}Sn (ppm)	278	119	98	−133
^{183}W (ppm)	−3393	−3220	−1463	−1411
$^{1}J_{WHyd}$ (Hz)	73	71		
$^{1}J_{WSn}$ (Hz)	1012	1326	947	1201
$^{1}J_{SnC}$ (Hz)	178	250	187	288
$^{2}J_{SnHyd}$ (Hz)	159	175		
$^{2}J_{SnCpC}$ (Hz)	5	b	5	*b*
$^{3}J_{SnCpH}$ (Hz)	8	10	6	7

[a] NMR chemical shifts and coupling constants in THF-d_8 at 298 K. [b] Not observed.

value as a useful predictor for solid state W−Sn bond length (r_{WSn}) in complexes of this type. Since the interpretation of these $^{1}J_{WSn}$ values would be complicated by the presence of multiple conformers in solution, this paper also describes the exploration of the conformational behavior of these complexes through X-ray crystallography and variable-temperature multinuclear NMR spectroscopy. These experimental results are coupled with DFT computational studies at the B3LYP/LANL2DZ level of theory to provide additional insight into the impact of the conformational behavior of this simple system on the correlation between $^{1}J_{WSn}$ and r_{WSn}.

Results

Synthesis. The compounds $Cp_2WHSnClR_2$ (**1a**, R = *t*-Bu; **1b**, R = Ph) were synthesized in procedures analogous to those used in the literature[2,3,10−14] for similar compounds, eq 1. After purification of the hydride complexes (**1a**,**b**) by recrystallization from THF/hexanes at −80 °C, heating in neat chloroform[15] at 45−50 °C resulted in formation of $Cp_2WClSnClR_2$ (**2a**,**b**) in high yield, eq 1. All four of these complexes were characterized completely, including satisfactory carbon and hydrogen elemental analyses. In a similar manner, the previously synthesized[16] compound $Cp_2WHSnPh_3$ (**4**) was also synthesized and fully characterized in this lab.

Multinuclear Variable-Temperature NMR Studies. Variable-temperature multinuclear NMR experiments were utilized to investigate the solution state structure of these complexes. Table 1 summarizes the ^{183}W chemical shifts, ^{119}Sn chemical shifts, and relevant one-, two-, and three-bond coupling constants to ^{119}Sn and ^{183}W. Several of these parameters exhibited temperature dependencies; the temperature dependence of the ^{119}Sn−^{183}W coupling constant in **1**, **2**, and **4** is illustrated in Figure 1. Furthermore, a correlation (R^2 = 0.87, Figure 2 and eq 2) exists between the solution state parameter $^{1}J_{WSn}$ and the crystallographically determined W−Sn bond length, r_{WSn}.

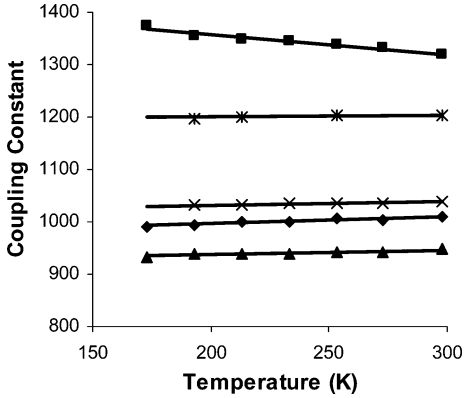

Figure 1. Temperature dependence of $^{1}J_{WSn}$ in **1a** (◆), **1b** (■), **2a** (▲), **2b** (*), **4** (×).

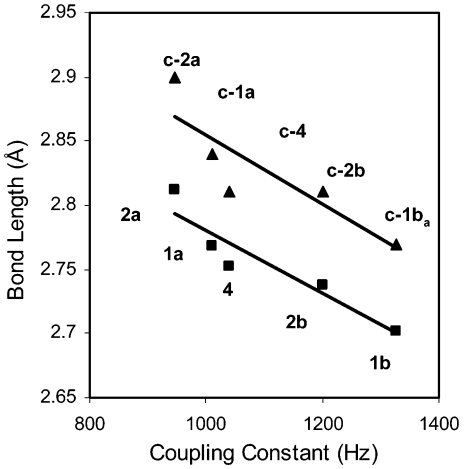

Figure 2. Bond length vs coupling constant for complexes **1**, **2**, and **4** (■ experimental bond length at 190 K, R^2 = 0.87; ▲ B3LYP/LANL2DZ bond length, R^2 = 0.75).

The statistical analysis for this correlation as well as a graphical representation of the confidence interval in the correlation is included as Supporting Information.

$$r_{WSn} = {}^{1}J_{WSn}\,(-2.4 \times 10^{-4}\ \text{Å/Hz}) + (3.02\ \text{Å}) \quad (2)$$

X-ray Studies. Compounds **1a**,**b**, **2a**,**b**, and **4** were characterized crystallographically, and details of these crystallographic studies are summarized in Table 2. ORTEP representations of **1a**, **1b**, and **4** are given in Figures 3a−5a along with structures from the DFT B3LYP/LANL2DZ calculations (Figures 3b−5b and 4c, see below), and ORTEP representations of **2a** and **2b** are available as Supporting Information. Pertinent bond lengths and angles are listed in Table 3 along with the corresponding values from the B3LYP/LANL2DZ calculations (see below). The dominant feature differentiating the structures of **1a** and **2a** from **1b** and **2b** is a change in the location of the substituents on the tin relative to the cyclopentadienyl rings. In **1a** and **2a**, the conformer adopted in the solid state has the Cl_{Sn} in a gauche orientation relative to the tungsten hydride (**1a**) or chloride (**2a**), while in **1b** and **2b** the chlorine is in an anti orientation.

Computational Studies. Molecular mechanics and semiempirical structures were calculated using the Wavefunction/Schrödinger program Titan.[17] Density

(15) Koloski, T. S.; Pestana, D. C.; Carroll, P. J.; Berry, D. H. *Organometallics* **1994**, *13*, 489−499.
(16) Perevozchikova, N. V.; Smirnov, A. S.; Sorokin, Y. A.; Kaplina, R. V.; Dodonov, V. A. *Zh. Obsch. Khim.* **1979**, *49*, 945.
(17) *Jaguar 3.5*; Schrodinger, Inc.: Portland, OR, 1998.

Table 2. Crystallographic Data

	1a	**1b**	**2a**	**2b**	**4**
empirical formula	$C_{18}H_{29}ClSnW$	$C_{22}H_{21}ClSnW$	$C_{18}H_{28}Cl_2SnW$	$C_{22}H_{20}Cl_2SnW$	$C_{28}H_{26}SnW$
fw	583.43	623.41	617.87	657.85	665.04
cryst description	orange block	orange block	dark red prism	dark red triangular plate	yellow prism
cryst size (mm)	0.25 × 0.36 × 0.36	0.12 × 0.20 × 0.28	0.31 × 0.33 × 0.36	0.33 × 0.32 × 0.03	0.16 × 0.24 × 0.18
cryst syst	monoclinic	monoclinic	monoclinic	orthorhombic	monoclinic
space group	$P2_1/n$	$P2_1/c$	$P2_1/c$	$Pna2_1$	$P2_1/c$
a (Å)	9.9297(20)	9.9519(20)	14.0810(14)	15.7779(15)	8.1625(8)
b (Å)	14.2323(28)	13.4168(27)	9.5502(10)	9.1602(9)	16.6601(17)
c (Å)	13.8325(28)	15.1608(30)	15.2488(15)	14.0138(14)	17.2325(17)
α (deg)	90	90	90	90	90
β (deg)	96.208(30)	104.227(30)	107.834(5)	90	99.078(5)
γ (deg)	90	90	90	90	90
V (Å^3)	1943.38(64)	1962.22(154)	1952.07(33)	2025.40(3)	2314.06(19)
Z	4	4	4	4	4
d(calcd, Mg/m^3)	1.99	2.11	2.10	2.16	1.91
abs coeff (mm^{-1})	7.330	7.268	7.436	7.175	6.058
F(000)	1111.7	1175.7	1175.7	1239.7	1271.7
θ range (deg)	2.5−27.5	3.2−27.5	3.2−27.5	2.6−27.5	2.8−27.5
no. of reflns	15929	16527	15457	14633	18822
no. of indep reflns	4452	4492	4457	4608	5304
no. of reflns obsd ($>4\sigma$)	3832	3943	4338	3742	4757
index ranges	$-12 \le h \le 12$ $-18 \le k \le 18$ $-17 \le l \le 17$	$-12 \le h \le 12$ $-17 \le k \le 17$ $-19 \le l \le 19$	$-18 \le h \le 18$ $-12 \le k \le 12$ $-18 \le l \le 19$	$-20 \le h \le 20$ $-8 \le k \le 11$ $-18 \le l \le 18$	$-10 \le h \le 10$ $-21 \le k \le 21$ $-22 \le l \le 22$
no. of data/restraints/params	4452/0/198	4492/0/230	4457/0/206	4608/11/236	5304/0/276
ext coeff	0.0022	0.0009	0.0049	not used	0.0014
goodness-of-fit on F^2	1.061	1.022	1.173	1.005	1.082
R indices (obsd data, $F_o > 4\sigma(F_o)$)	R_1 0.035, $wR_2 = 0.067$	R_1 0.020, $wR_2 = 0.039$	R_1 0.019, $wR_2 = 0.047$	R_1 0.0388, $wR_2 = 0.0844$	R_1 0.022, $wR_2 = 0.048$
R indices (all data)	$R_1 = 0.044$, $wR_2 = 0.070$	$R_1 = 0.026$, $wR_2 = 0.041$	$R_1 = 0.020$, $wR_2 = 0.047$	$R_1 = 0.057$, $wR_2 = 0.092$	$R_1 = 0.027$, $wR_2 = 0.050$
largest diff peak and hole (e Å^{-3})	4.305/−3.825	0.738/−0.745	0.848/−1.507	1.70/−1.17	0.832/−1.111

Table 3. Pertinent Bond Distances (Å) and Angles (deg) of Complexes 1, 2, and 4

	1a	**1a** (calc)	**1b**	**1b** anti (calc)	**1b** gauche (calc)	**2a**	**2a** (calc)	**2b**	**2b** anti (calc)	**4**	**4** (calc)
					Bond Lengths						
W−Sn	2.7681(8)	2.84	2.7020(6)	2.77	2.78	2.8113(4)	2.90	2.7376(7)	2.81	2.7517(3)	2.81
Sn−Cl	2.464(2)	2.52	2.467(1)	2.49	2.49	2.4379(9)	2.51	2.424(3)	2.49	2.170(3)[b]	2.17[b]
Sn−C^A	2.216(6)	2.22	2.160(3)	2.16	2.15	2.233(3)	2.23	2.141(9)	2.15	2.178(3)	2.17
Sn−C^B	2.220(6)	2.22	2.164(3)	2.16	2.15	2.227(3)	2.23	2.152(8)	2.15	2.178(3)	2.17
W−X	1.83(7)	1.70	1.57(3)	1.71	1.70	2.4754(8)	2.56	2.495(2)	2.58	1.54(4)	1.70
					Angles						
X−W−Sn	73.0(2.2)	73.3	75.3(11)	74.5	74.6	84.18(2)	80.4	75.65(5)	75.1	77.0(15)	72.2
W−Sn−Cl	112.72(4)	110.1	110.18(4)	110.9	110.5	110.27(2)	110.5	111.18(7)	104.9	116.4(1)[b]	116.0[b]
W−Sn−C^A	117.04(17)	116.5	124.97(9)	118.2	118.2	118.67(7)	113.6	118.3(2)	119.7	113.0(1)	113.4
W−Sn−C^B	117.76(16)	118.1	119.45(9)	118.2	119.3	118.65(7)	120.8	117.7(2)	119.7	116.2(1)	113.4
C^A-Sn−C^B	113.94(23)	113.0	103.10(11)	105.7	105.8	110.74(11)	112.0	106.7(3)	107.6	103.4(1)[b]	104.6[b]
Cl−Sn−C^A	96.21(16)	98.8	97.04(8)	100.5	100.0	94.36(8)	97.7	99.1(2)	100.6	102.5(1)[b]	104.1[b]
Cl−Sn−C^B	94.30(17)	96.1	96.28(8)	100.5	100.0	99.35(8)	98.3	101.0(2)	100.6	103.6(1)	104.1
$\sum\omega$[a]	51.95	43.80	58.18	40.60	42.2	45.62	41.90	40.38	44.70	36.10	30.00
					Dihedral Angles						
X−W−Sn−Cl	81.1(23)	73.5	166.4(11)	180	50.6	87.71(3)	79.4	170.28(10)	180	178.2(15)	180

[a] Reference 13. [b] In **4**, carbon (C^C) of phenyl anti to hydride instead of Cl.

functional theory calculations[18] were done using Gaussian '03. Initial structures for **1a** and **1b** were minimized using the Merck Molecular Mechanics Force Field[19] (MMFF94) followed by the PM3/d semiempirical routine. Conformational space for the W−Sn compounds was explored at the PM3/d level by utilizing a dihedral driver to vary the dihedral angle X−W−Sn−Cl (X = H, Cl). The structures located at minima were then selected, the geometric coordinates transferred to Gaussian, and DFT calculations performed using the hybrid functional B3LYP and the basis set[20] LANL2DZ. Convergence parameters for the geometry optimization were set to very tight,[21] and the ultrafine grid[22] was used for calculation of the two-electron integrals. Following initial geometry optimization using an estimated Hessian matrix, final optimizations were based upon calculated analytical force constants using the harmonic oscillator approximation. The final vibrational frequencies were checked to ensure that all values were nonimaginary.

To obtain better values for the potential energy surface for rotation around the W−Sn bond, a coordinate scan driving the X−W−Sn−Cl dihedral (X = H, Cl) at the B3LYP/LANL2DZ level was repeated for compounds **1a** and **1b** (Figure 6) and **2a** and **2b** (Supporting Information). Minimizations of transition states to obtain accurate energies for the bond rotation proved

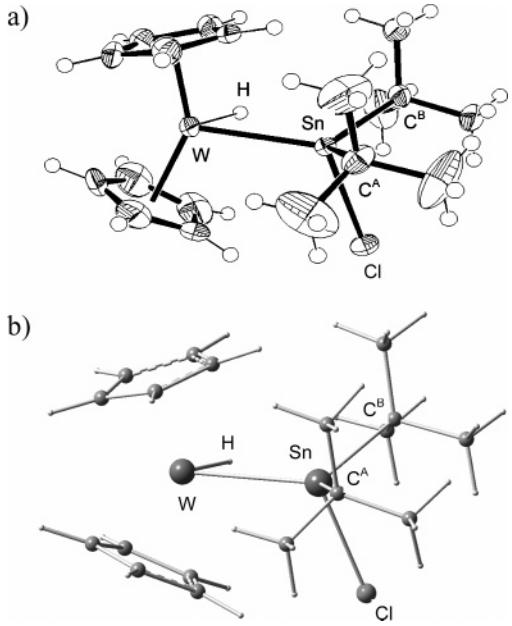

Figure 3. (a) ORTEP representation of crystal structure of $Cp_2WHSnClt Bu_2$ (**1a**). (b) Ball-and-stick representation of B3LYP/LANL2DZ calculated structure of **1a**.

to be computationally extremely expensive for these large structures and were abandoned.

Graphic representations of the global energy minima for **1a** and **4** are depicted in Figures 3b and 5b, and pertinent bond lengths and bond angles are summarized in Table 3. For complexes **1b** and **2b**, two conformational isomers were examined, one in which the X−W−Sn−Cl dihedral angle is essentially 180° (anti orientation) and one in which it has assumed a gauche orientation (approximately 50°). These structures for **1b** are depicted in Figure 4b (anti-**1b**) and 4c (gauche-**1b**). The analogous structures for **2b** are included in the Supporting Information. The relative energy difference between the anti and gauche forms for **1b** is only 0.6 kcal/mol, within the expected error for DFT calculations at this level. The energy difference between the anti and gauche forms of **2b** is slightly higher, at 4.5 kcal/mol. A plot of calculated W−Sn bond lengths vs $^1J_{WSn}$ is depicted in Figure 2 ($R^2 = 0.75$). Only one unique conformational isomer for **1a** corresponding to a dihedral angle (H−W−Sn−Cl) of 73.5° was found computationally. In contrast, upon investigation of the energy surface for **2a**, a second energy minimum corresponding to a dihedral angle of 156.6° was found. After full minimization of this second conformer, a difference in energy between the two conformations **2a** (79°) and **2a** (157°) was determined to be 0.3 kcal/mol. Computational details of these calculations are included as Supporting Information.

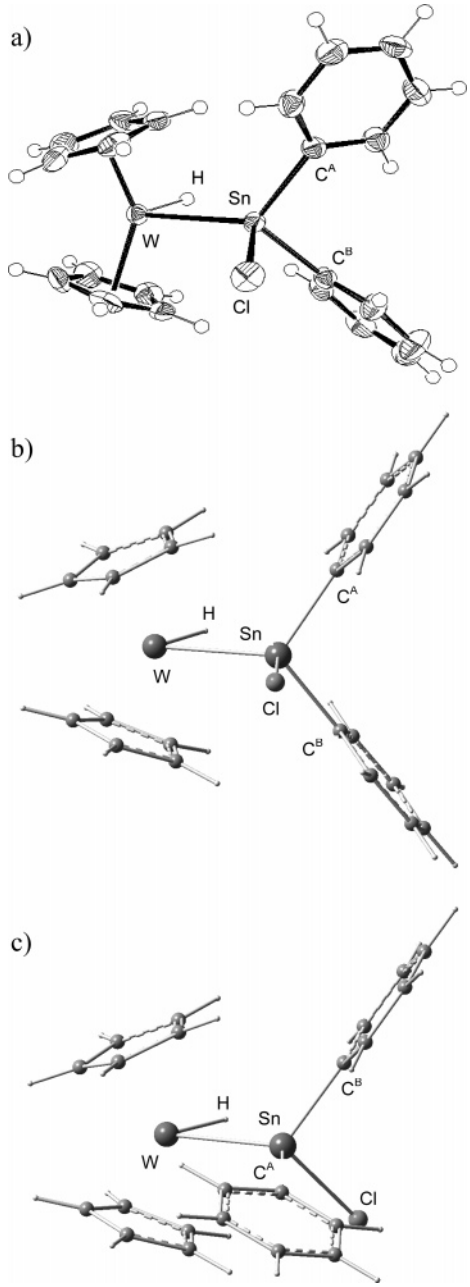

Figure 4. (a) ORTEP representation of crystal structure of $Cp_2WHSnClPh_2$ (**1b**). (b) Ball-and-stick representation of B3LYP/LANL2DZ calculated structure of anti-**1b**. (c) Ball-and-stick representation of B3LYP/LAN2LDZ calculated structure of gauche-**1b**.

Discussion

During the investigation of the chemical reactivity of complexes **1** and **2**, the current study was undertaken in order to investigate the relationship between solution

(18) Frisch, M. J.; Trucks, G. W.; Schlegel, H. B.; Scuseria, G. E.; Robb, M. A.; Cheeseman, J. R.; J. A. Montgomery, J.; Vreven, T.; Kudin, K. N.; Burant, J. C.; Millam, J. M.; Iyengar, S. S.; Tomasi, J.; Barone, V.; Mennucci, B.; Cossi, M.; Scalmani, G.; Rega, N.; Petersson, G. A.; Nakatsuji, H.; Hada, M.; Ehara, M.; Toyota, K.; Fukuda, R.; Hasegawa, J.; Ishida, M.; Nakajima, T.; Honda, Y.; Kitao, O.; Nakai, H.; Klene, M.; Li, X.; Knox, J. E.; Hratchian, H. P.; Cross, J. B.; Adamo, C.; Jaramillo, J.; Gomperts, R.; Stratmann, R. E.; Yazyev, O.; Austin, A. J.; Cammi, R.; Pomelli, C.; Ochterski, J. W.; Ayala, P. Y.; Morokuma, K.; Voth, G. A.; Salvador, P.; Dannenberg, J. J.; Zakrzewski, V. G.; Dapprich, S.; Daniels, A. D.; Strain, M. C.; Farkas, O.; Malick, D. K.; Rabuck, A. D.; Raghavachari, K.; Foresman, J. B.; Ortiz, J. V.; Cui, Q.; Baboul, A. G.; Clifford, S.; Cioslowski, J.; Stefanov, B. B.; Liu, G.; Liashenko, A.; Piskorz, P.; Komaromi, I.; Martin, R. L.; Fox, D. J.; Keith, T.; Al-Laham, M. A.; Peng, C. Y.; Nanayakkara, A.; Challacombe, M.; Gill, P. M. W.; Johnson, B.; Chen, W.; Wong, M. W.; Gonzalez, C.; Pople, J. A. *Gaussian 03W*, Revision C.1; Gaussian, Inc.: Pittsburgh, PA, 2003.
(19) Halgren, T. A. *J. Comput. Chem.* **1996**, *17*, 490.
(20) Hay, P. J.; Wadt, W. R. *J. Chem. Phys.* **1985**, *82*, 299.
(21) Units: maximum force = $2 \times e^{-6}$ Hartree/bohr, rms forces = $1 \times e^{-6}$ Hartree/bohr, max displacement = $6 \times e^{-6}$ bohr, rms displacement = $4 \times e^{-6}$ bohr.
(22) A pruned (99 590) grid was utilized; tungsten defaults to an unpruned grid.

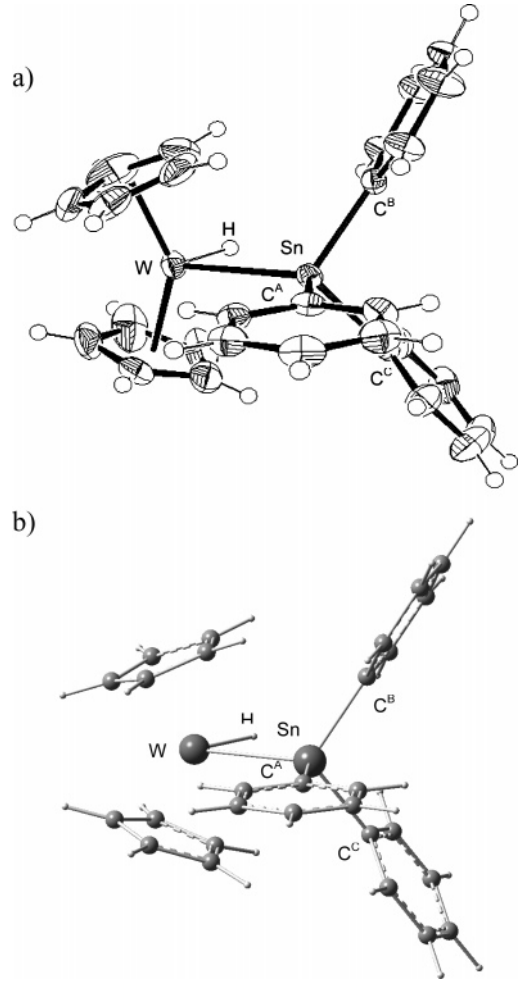

Figure 5. (a) ORTEP representation of crystal structure of $Cp_2WHSnPh_3$ (**4**). (b) Ball-and-stick representation of B3LYP/LANL2DZ calculated structure of **4**.

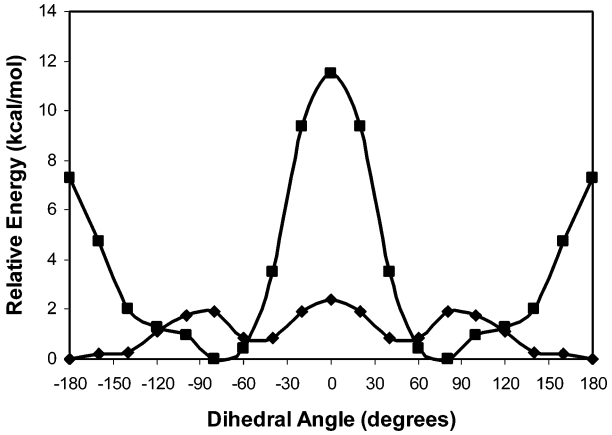

Figure 6. Calculated (B3LYP/LANL2DZ) energy barrier for interconversion of two rotameric minima of **1a** (■) and **1b** (◆). Dihedral angle illustrated is H−W−Sn−Cl.

state NMR parameters in comparison to the solid state structures. The observation of different solid state conformations for **1a** and **1b** (or **2a** and **2b**) and the correlation between the solid state r_{WSn} and the solution state $^1J_{WSn}$ indicated that a careful study of these complexes, including their conformational behavior, might yield the tungsten−tin coupling constant as a useful diagnostic tool for the prediction of *solid state* tungsten-stannyl complexes.

Solid State Structures of 1 and 2. The solid state structures of $Cp_2WHSnClR_2$ (**1**, Figures 3a, 4a), $Cp_2WClSnClR_2$ (**2**, figures in Supporting Information), and $Cp_2WHSnPh_3$ (**4**, Figure 5a) resemble those of previously synthesized compounds that have already been thoroughly described.[2,12,13] The following discussion concentrates on the most striking difference between the *tert*-butyl derivatives **1a** and **2a** and their phenyl analogues **1b** and **2b**, namely, a change in the solid state conformational preference. The sterically more demanding *tert*-butyl substituents in **1a** and **2a** cause the tin to rotate so these groups essentially occupy the equatorial plane between the two cyclopentadienyl (Cp) groups, placing the chlorine substituent in an eclipsing interaction with one of the Cp groups. This is accompanied by an opening to 114° of the C−Sn−C angle between the two *tert*-butyl groups. In contrast, in **1b** and **2b**, the chlorine occupies the position essentially anti to the hydride (dihedral angle = 166.4° for **1b** and 170.3° for **2b**), and the two phenyl groups rotate to present their faces to the two cyclopentadienyl groups. By comparison, in this structure the C−Sn−C angle of the two phenyl groups is only 103°.

Furthermore, these structural differences are accompanied by changes in the tungsten−tin bond length (Table 3, Figure 2). The difference in bond lengths observed could be rationalized by a variety of explanations. For instance, the longer bond in **1a** and **2a** as compared to **1b** and **2b** could be due to (1) a change in the hybridization of the tin resulting in greater s-character in the tin−tungsten bond in the phenyl cases, (2) a simple increase in steric repulsion due to the larger size of the *tert*-butyl substituents, or (3) an additional π-back-bonding interaction between a filled tungsten orbital and a low-lying empty tin-based orbital in the diphenyl tin compounds **1b** and **2b**. The bond lengthening that occurs upon substitution of the tungsten hydride for a chloride on going from **1a** to **2a** and **1b** to **2b** might be explained by (1) changes in the hybridization of the tungsten resulting in less s-character in the tungsten−tin bond in the chlorine cases, (2) an increase in Coulombic repulsion between Cl_W and Cl_{Sn}, or (3) a decrease in the ability of the tungsten center to π-back-bond to the tin upon chlorine substitution.

Turning first to changes in the substitution at the tin center, Bulychev and co-workers[13] examined the series of compounds $Cp_2MoHSnCl_nMe_{3-n}$. In these studies, the molybdenum tin bond lengthens upon substitution of methyl groups for chlorine. While this could be explained by either a π-back-bonding argument or a change in hybridization argument, Bulychev argued that changes in the bond angles around the tin center indicate that the latter is operative. Furthermore, this argument was supported by Mössbauer spectroscopy, which indicates that the increase in bond length is concomitant with the tin center becoming increasingly sp^3 hybridized. The hybridization argument was also supported by NMR evidence,[13] in which a decrease in the two-bond scalar coupling constant between the tin and the methyl protons ($^2J_{HSn}$) upon methyl substitution is observed. Bulychev's work with stannyl ligands stands in contrast with results found by Berry and coworkers[15] regarding comparable silicon analogues. In the case of silicon, Berry reported that π-back-bonding

between the transition metal center and the silicon occurs, as evidenced by a lengthening of the Si−Cl bond relative to typical values and by ^{29}Si NMR chemical shifts indicative of partial silylene character.

The structural factors influencing complexes **1** and **2** appear to be more complex than those of the complexes studied by Bulychev. For instance, Bulychev measured[13] the extent of tin hybridization by examining the bond angles around the tin center, finding upon methyl substitution (and thus Mo−Sn bond lengthening) increases in the W−Sn−X bond angles with concomitant decreases in the X−Sn−X bond angles (X = Me, Cl). In contrast, presumably due to more drastic steric changes, a consistent trend is not available in complexes **1**, **2**, and **4** (Table 3).

To describe numerically the apparent hybridization at the tin center, Bulychev[13] used the value $\sum\omega$ (eq 3), the sum of the absolute difference between the six bond angles around the tin and the idealized tetrahedral angle of 109.5°. Strong deviation from the idealized

$$\sum\omega = \sum_{i,j}|\angle(\mathrm{X}_i - \mathrm{Sn} - \mathrm{Y}_j) - 109.5| \qquad (3)$$

tetrahedral angle is indicated by an increasing $\sum\omega$ value, with limiting values of 0° when completely hybridized (six 109.5° angles) or 106° when completely unhybridized (three 90° and three 125.3° bond angles).[13,23,24] The $\sum\omega$ values for complexes **1**, **2**, and **4** are included in Table 3. By this comparison of bond angles, complex **2b** has $\sum\omega = 40.47$, indicating it is more sp^3 hybridized than either **1a** ($\sum\omega = 51.95$) or **2a** ($\sum\omega = 45.62$) and thus should have less s-character in the W−Sn bond and therefore a longer bond; however, **2b** has a shorter W−Sn bond length than either **1a** or **2a**. Similarly, by this criterion, complex **4** is substantially more hybridized than any other complex and yet has an intermediate W−Sn bond length. These deviations from the trends found by Bulychev are not unexpected. Whereas Bulychev investigated a well-defined series of compounds with small, sterically undemanding substituents, the steric demands of the organic substituents in complexes **1** and **2** are dominating the structural behavior at the tin center. In the current situation, it appears that the differences between **1a** and **1b** and between **2a** and **2b** are primarily steric in origin and that changes in the hybridization of the tin center are not substantially influencing the W−Sn bond length.

While it is clear that hybridization changes are less important than the steric demands of the *tert*-butyl ligands, determining if significant π-bonding is occurring in these complexes is more difficult. In agreement with both Bulychev[13] and Schubert,[2] the similarity of the Sn−Cl bond lengths in **1a** and **1b** would indicate that no significant π-back-bonding by the filled tungstenocene a_1 orbital into the Sn−Cl σ^* orbital occurs. While in **1b** the Sn−Cl σ^* orbital is oriented appropriately for the π-back-bonding interaction, in **1a** the antibonding orbital is not aligned appropriately (Figure 7). There is, however, a shortening in the Sn−Cl bond length in complexes **2a** and **2b** relative to **1a** and **1b**.

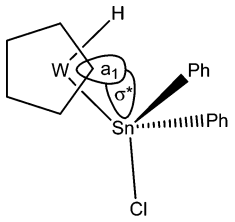

$Cp_2WHSnClPh_2$ (**1b**)
$r_{W\text{-}Sn}$ = 2.7020(6)
$r_{Sn\text{-}Cl}$ = 2.467(1)

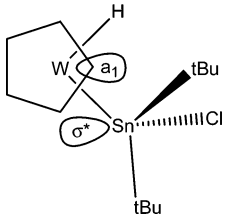

$Cp_2WHSnCl^tBu_2$ (**1a**)
$r_{W\text{-}Sn}$ = 2.7681(8)
$r_{Sn\text{-}Cl}$ = 2.464(2)

Figure 7. Orientation of the Sn−Cl σ^* orbital relative to the a_1 tungstenocene fragment orbital in $Cp_2WSnClPh_2$ (**1b**) and $Cp_2WHSnCl^tBu_2$ (**1a**). Lengthening of the Sn−Cl bond is expected in **1b** relative to **1a** if this orbital interaction is important. No significant difference in Sn−Cl is observed.

Additionally, there is a W−Sn bond lengthening of **2a** relative to **1a** and of **2b** relative to **1b**. This could be explained by π-back-bonding from two different filled tungsten-based orbitals in **1a** and **1b** that is reduced in **2a** and **2b** due to changes in tungsten electron density. It was hoped that DFT calculations might assist in determining the origin of these changes; however, as described below, the DFT calculations provide no further insight.

NMR and VT-NMR Studies of Complexes 1 and 2. Correlations between solid state structural parameters and solution NMR parameters, such as chemical shift and coupling constants, have been used extensively in the literature to understand organometallic systems[25] and have been used specifically in studies related to the current investigation.[2,13,15] Bulychev[13] found a correlation between the Mo−Sn bond length and the magnitude of the two-bond coupling constant of the tin and methyl protons ($^2J_{SnH}$) in the series $Cp_2MoHSnCl_nMe_{3-n}$. However, complexes **1**, **2**, and **4** are not amenable to such a study due to the changes in organic substituents on the tin. On the other hand, as shown in Figure 2, there is a correlation ($R^2 = 0.87$) between the observed solid state bond lengths (r_{WSn}) and the observed one-bond W−Sn scalar couplings ($^1J_{WSn}$) for complexes **1**, **2**, and **4**. This correlation stands in contrast to the analogous silicon systems studied by Berry and coworkers[15] that demonstrated there was no simple correlation between $^1J_{WSi}$ and the silicon bond length r_{WSi} in a series of tungstenocene silyl hydride and bis-silyl complexes. Given the modest scatter in the correlation data and the fact that Berry observed fluxional behavior involving rotation about the W−Si bond, a study investigating the dynamic behavior of complexes **1**, **2**, and **4** was deemed necessary to understand better the relationship between r_{WSn} and $^1J_{WSn}$.

To this end, variable-temperature ^{1}H and ^{119}Sn NMR spectroscopy experiments were undertaken for **1**, **2**, and **4** to probe for evidence of fluxional processes in these complexes. The ^{1}H NMR spectra for all five compounds

(23) Huheey, J. E. *Inorganic chemistry: Principles of structure and reactivity*, 3rd ed.; Harper & Row: New York, 1983.

(24) Page 117 of ref 23 provides a graphic description of the bond angles around an unhybridized atom.

(25) Mann, B. E. *Spectrosc. Prop. Inorg. Organomet. Compd.* **1997**, *30*, 1−209.

exhibit little change over a range of temperatures from 298 to 173 K. Both show some broadening at the final low temperature of 173 K; however, this does not appear to be due to a fluxional process but rather from changes in the rate of molecular tumbling due to changes in solvent viscosity. Similarly, the ^{119}Sn spectra show no indication of broadening due to a dynamic process. As tin NMR chemical shifts are quite sensitive to minor changes in structure, the absence of broadening indicates either a single possible conformer (or equivalent conformers) or extremely fast exchange between existing conformers. All five complexes studied show similar substantial changes in chemical shift over the temperature range studied; however, tin chemical shifts are typically quite temperature dependent, so this observation provides little probative value.

However, examination of the temperature dependence of $^1J_{WSn}$ in these complexes does indicate that **1b** exhibits different temperature dependence than the other four compounds **1a**, **2a**, **2b**, and **4**, potentially suggesting different fluxional behavior in the case of **1b**. As depicted in Figure 1, the $^1J_{WSn}$ value for **1b** has an inverse temperature dependence with a slope of -0.35 ± 0.09 Hz/K (95% confidence limits), while $^1J_{WSn}$ for **1a**, **2a**, and **4** have only a very slight direct dependence on the temperature (**1a**: $m = 0.15 \pm 0.05$ Hz/K, **2a**: $m = 0.09 \pm 0.04$ Hz/K; **4**: $m = 0.08 \pm 0.02$ Hz/K). The temperature dependence of **2b** is not statistically significant, nor is there a statistically significant difference in the slopes of **1a**, **2a**, and **4**. At this point, insufficient data are available to interpret the weak effect that seems to be operative in **1a**, **2a**, and **4**. It is interesting to note that the more substantial temperature dependence of **1b** is also opposite in sign from the temperature dependence of the other four. While not conclusive, this temperature dependence exhibited by **1b** might be explained by a change in the relative populations of two low-lying conformations each with a different $^1J_{WSn}$. Because the barriers to conformational interconversion in these complexes were too low to allow differentiation of conformers by VT-NMR studies, density functional theory calculations were undertaken to estimate the relative energies of the various conformers of **1**, **2**, and **4** to determine if the hypothetical difference in conformational behavior of **1b** relative to the other complexes was reasonable.

Calculated Structures. The DFT calculations carried out at the B3LYP/LANL2DZ level of theory generated geometry-optimized structures matching the crystal structures both in terms of gross structure and in terms of some structural details (Figures 3−5, Table 3). For complexes **1b** and **2a**, which have two energetically similar conformations, the conformational isomer closest in X−W−Sn−Cl dihedral angle was chosen to compare to the X-ray structures. As previously noted in similar calculations,[26,27] the transition metal−tin bond length was overestimated in these calculations, but the general trend observed in complexes **1** and **2** and even the relative differences are reflected accurately. The geometry around the tin center is correct in terms of the gross structure; for instance, the calculations adequately predict the difference in conformations due to the change from ^{t}Bu to Ph substituents in **1a** and **1b**. Differences in the details may be due in part to crystal packing influences. For example, in **1b**, the W−Sn−C^A angle is predicted to be much smaller than observed in the crystal structure, and in **1a** and **2a**, the X−W−Sn−Cl dihedral angle is predicted to be more acute than actually observed. Similarly, the predicted structures are much more symmetrical than observed in the crystal; the X−W−Sn−Cl dihedral angle is predicted to be exactly 180° in both **1b** and **2b**.

Compounds **1** and **2** show low energy barriers to full rotation around the W−Sn single bond, in keeping with the VT-NMR data reported above. In addition, as can be seen in Figure 6, the potential energy surfaces near the minima of **1a** and **1b** are quite flat with respect to small amounts of rotation around the W−Sn bond. Consistent with this observation, the force constant calculations for **1b** and **2b** predict extremely low frequencies for the torsion mode involving rotation about the W−Sn bond in both the anti and gauche conformations (e.g., 6 cm^{-1} for **1b**-anti and 15 cm^{-1} for **1b**-gauche). The predicted frequencies for the same modes in **1a** and **2a** are higher (e.g., 27 cm^{-1} for **1a**), due to the increased steric repulsion between the ^{t}Bu and Cp moieties, but are still the lowest frequency modes of the molecule. These theoretical findings are consistent with the observed minor deviations in the crystal structures from the theoretically predicted structures. For example, minor changes in the X−W−Sn−Cl dihedral angle would result in a small decrease in the stability of an individual molecule that is compensated by intermolecular packing forces.

The crystallographic studies discussed above found minor differences in the Sn−Cl bond length that raised the possibility of a change in the electronic nature of the W−Sn interaction upon substitution of a chloride for the hydride on the tungsten. However, the relative differences of the Sn−Cl bond lengths of these complexes, including the difference between **1a** and **1b** and the difference between complexes **1** and **2**, are not accurately predicted by the B3LYP/LANL2DZ calculations. This failure precludes any hope that these DFT calculations can help explain the observed small differences in the Sn−Cl bond length in the crystal structures.

As shown in Figure 6, the calculated potential energy surface for rotation about the W−Sn bond is dramatically different for $Cp_2WHSnCl^tBu_2$ (**1a**) as compared to $Cp_2WHSnClPh_2$ (**1b**). Whereas **1a** has two equivalent conformational minima, **1b** has a third conformation that is the global minimum. In fact, the corresponding geometry in **1a** is actually one of the transition states between the two minima. The calculations also predict that there is a very small energy difference[28] between the anti and gauche conformations of **1b** (0.6 kcal/mol), but a greater difference in energy between the anti and gauche conformations of **2b** (4.5 kcal/mol). There are also two energetically similar conformational isomers

(26) Zhang, L.; Zhang, Y.; Tao, H.; Sun, X.; Guo, Z.; Zhu, L. *THEOCHEM* **2002**, *617*, 87−97.

(27) Cundari, T. R., Ed. *Computational organometallic chemistry*; Marcel Dekker: New York, 2001.

(28) This energy difference is based upon the difference in the calculated energies of anti- and gauche-**1b** (or **2b**) at 298.15 K after correction for the fact that there should be no entropic contribution due to differences in the calculated frequency of the hindered rotation around the W−Sn bond; see the explanation of this correction in the Supporting Information for further details.

of **2a** 79° and **2a** 157° separated by a small barrier (Supporting Information). At this point, the origin of the difference in the energy surfaces of **1a** and **2a** is suspected to be due to the decrease in the steric constraints of the *tert*-butyl groups due to the lengthening of the W−Sn bond. The necessary, thorough analysis of the origin of the differences in these potential energy surfaces is beyond the scope of the current paper and will be the subject of additional studies. Three conformations are accessible to $Cp_2WHSnPh_3$ (**4**); however, due to symmetry, all three conformations of **4** are equivalent in energy.

The two different conformational isomers available to **1b** may explain the observation that the $^1J_{WSn}$ coupling of **1b** shows a dependence on temperature, although similar (unobserved) behavior for **2a** might also be expected. Compounds **1b** and **2a** are unique in the sense that they are the only compounds that would be expected to exhibit dependence of $^1J_{WSn}$ on temperature due to a conformational equilibrium. For example, with only ~0.6 kcal/mol difference in energy[29] between anti-**1b** and gauche-**1b**, a relatively large change in conformer population occurs between 170 (83:17) and 300 K (63:37). In contrast, **1a** and **4** both have equivalent conformers and **2b** has a large energy gap between the gauche and anti conformations. The absence of a similar effect for **2a** could be due to similar coupling constants for the two isomers or the lack of a temperature dependence on the populations due to essentially equivalent energies. However, it is also possible that the temperature dependence observed in **1b** arises from an additional unidentified factor that does not affect the other compounds.

Limitations of the Correlation between $^1J_{WSn}$ and r_{WSn}. The coupling constant $^1J_{WSn}$ has the potential to be useful as a solution parameter for the prediction of the solid state tungsten tin bond length, r_{WSn}. However, in addition to the inherent inaccuracies in a correlation with $R^2 = 0.87$, the current study has indicated that further pitfalls must be avoided. In this particular study, there appears to be the potential for variability in the correlation due to conformational changes, and in other complexes the effect of such changes may be more dramatic. Furthermore, it is clear from the comparison of the calculated structures of **1**, **2**, and **4** to the crystallographically determined structures that variations in the solid state geometrical parameters due to crystal packing are likely to affect the solid state bond length. Furthermore, solvent effects appear to be important as the coupling constant in **2a** drops from 947 Hz in THF-d_8 to 882 Hz in $CDCl_3$.

Conclusion

The tungstenocene complexes $Cp_2WHSnClR_2$ (R = ^{t}Bu (**1a**), Ph (**1b**)) and $Cp_2WClSnClR_2$ (R = ^{t}Bu (**2a**), Ph (**2b**)) provide insight into the nature of the static and dynamic behavior of the W−Sn bond. As expected, the bulky *tert*-butyl groups play a large role in forcing **1a** and **2a** to adopt a single conformer that minimizes steric repulsion between the Cp groups and ^{t}Bu groups. It appears that this steric effect outweighs any changes in tin hybridization in controlling the W−Sn bond length, in contrast to previous studies with much smaller organic substituents. In the case of phenyl substituents, **1b** and **2b** are able to adopt multiple conformers, although both prefer the same in the solid state. A correlation exists between the solution state NMR parameter $^1J_{WSn}$ and the solid state crystallographically determined W−Sn bond length. While this correlation may be useful in future studies, deviations due to conformational behavior may occur that have more drastic effects than the conformational behavior observed here did, and therefore, caution should be employed in using it to predict solid state structure. Further studies are underway with **1** and **2** to examine the solution chemistry of these species.

Experimental Section

General Comments. All procedures were carried out under an inert atmosphere of dry argon using standard Schlenk line techniques or in an M. Braun inert atmosphere glovebox. Glassware was dried for >20 min prior to use in an oven heated to 120 °C. Solvents (CH_2Cl_2, hexanes, toluene) for reactive chemistry were predried using 4 Å molecular sieves, sparged with gaseous N_2, and treated by passage through a column of activated alumina.[30] Anhydrous/O_2-free THF (without stabilizer) and Et_2O (with 2,6-di-*tert*-butyl-4-methylphenol stabilizer) were purchased directly from Aldrich and used with no further purification. $CHCl_3$ was dried by treatment with activated 4 Å molecular sieves, followed by cannula transfer and degassing using three freeze−pump−thaw cycles on a Schlenk line. NMR solvents were dried and degassed by stirring over CaH_2 followed by vacuum transfer to a storage vessel. THF-d_8 and C_6D_6 were further dried by stirring over Na/benzophenone. Collidine was distilled under Ar prior to use. Tungstenocene dihydride (**3**) was synthesized according to literature methods[31] or purchased from Aldrich Chemicals and used without further purification. The literature compound hydrido-bis(cyclopentadienyl)tungsten triphenylstannane (**4**) was synthesized in a manner similar to **1a** and **1b**, and details of this synthesis are included in the Supporting Information. All other reagents were purchased from Aldrich Chemicals and used with no further purification. ^{1}H, ^{13}C{^{1}H}, ^{119}Sn{^{1}H}, and ^{183}W{^{1}H} NMR spectra were obtained on a Bruker DRX 400 MHz NMR spectrometer. Proton and carbon spectra were referenced to NMR solvent peaks (ppm): C_6D_5H at 7.15 (^{1}H), 128.0 (^{13}C); $CHCl_3$ at 7.25 (^{1}H), 77.0 (^{13}C); d_7-THF at 3.58 (^{1}H), 67.57 (^{13}C). ^{119}Sn{^{1}H} NMR spectra were referenced externally to Me_4Sn (0) at 298 K; ^{183}W chemical shifts acquired through one-dimensional ^{183}W{^{1}H} spectra (**2a**, **2b**) or ^{1}H{^{183}W} gs-HMQC experiments (**1a**, **1b**, **4**) were referenced[32] externally to Cp_2WH_2 at −3550 (^{183}W) at 298 K. Mid- (4000−600 cm^{-1}) and far-IR (600−100 cm^{-1}) spectra were recorded on a Nicolet Nexus 670 FT-IR using KBr (mid) or polyethylene (far) pellets. Mass spectral data were obtained using a Hewlett-Packard 5989B quadrupole mass spectrometer with direct insertion inlet with ions indicated by the most intense peak within a given ion's isotopic envelope. Ion identity was determined by comparison to calculated isotopic patterns. Elemental analyses were performed at the Micro-Mass Facility at the College of Chemistry, University of California−Berkeley, under inert atmosphere. X-ray diffraction data were recorded in the Department of Chemistry X-ray facility at the University of Iowa.

(29) This simple argument is further complicated should there be a temperature dependence to $\Delta\Delta H$ or $\Delta\Delta S$; however, since the small energy differences indicated by the calculations are within the expected margin of error, it seems unwise to extend the analysis.

(30) Alaimo, P. J.; Peters, D. W.; Arnold, J.; Bergman, R. G. *J. Chem. Educ.* **2001**, *78*, 64.

(31) Green, M. L. H.; McCleverty, J. A.; Pratt, L.; Wilkinson, G. *J. Chem. Soc., IV* **1961**, 4854−4859.

(32) Mann, B. E. In *Annual Reports on NMR Spectroscopy*; Webb, G. A., Ed.; Academic: San Diego, 1991; Vol. 23, pp 141−207.

Synthesis of Hydridobis(cyclopentadienyl)tungsten-di-*tert*-butyltin Chloride ($Cp_2WHSnCl^tBu_2$, 1a). With constant stirring, a 50 mL THF solution containing 1.122 g (3.55 mmol) of tungstenocene dihydride was added by cannula over a 15 min period to a second 50 mL of THF solution of 1.086 g (3.57 mmol) of di-*tert*-butyltin dichloride and 3.0 mL (22.6 mmol) of collidine. During this addition the yellow tungstenocene solution turns a light orange color and a light-colored precipitate forms. This reaction mixture is stirred for a further 10 min, during which time additional precipitate forms. The supernatant was then transferred to a second flask by cannula filtration, and the solvent was removed in vacuo. The resulting orange solid was extracted with 2 × 30 mL of 1:1 hexanes/THF, separated by cannula filtration from additional precipitate, and the solvent was removed in vacuo, producing a light orange solid. Recrystallization from THF/hexanes (∼1:10) produced 1.52 g (2.61 mmol, 73%) of spectroscopically pure **1a**. A similar synthetic procedure gave analytically pure material after double recrystallization from THF/hexanes. ^{1}H NMR (THF-d_8): δ −12.62 (s, 1H, $J_{H^{119}Sn}$ = 159 Hz, J_{HW} = 73 Hz, W*H*), 1.23 (s, 9H, $J_{H^{119}Sn}$ = 59 Hz, ^{t}Bu), 4.76 (s, 10H, $J_{H^{119,117}Sn}$ = 8 Hz, Cp). ^{13}C{^{1}H} NMR (THF-d_8): δ 38 ($J_{C^{119}Sn}$ = 178 Hz, J_{CW} = 8 Hz, Sn-*C*), 74 ($J_{C^{119}Sn}$ = 5 Hz, Cp), 32 ($J_{C^{119}Sn}$ = 11 Hz, *C*H$_3$). ^{119}Sn{^{1}H} NMR (THF-d_8): δ 278 ($J_{Sn^{183}W}$ = 1012 Hz). ^{183}W NMR (HMQC, THF-d_8): δ −3393. IR (KBr, cm^{-1}): ν (WH stretch) 1915 (m). IR (polyethylene pellet, cm^{-1}): ν (SnCl stretch) 275 (s). Anal. Calcd for $C_{18}H_{29}WSnCl$: C, 37.06; H, 5.01. Found: C, 37.22; H, 5.06.

Synthesis of Hydridobis(cyclopentadienyl)tungsten-diphenyltin Chloride ($Cp_2WHSnClPh_2$, 1b). With constant stirring, a 50 mL THF solution containing 1.00 g (3.16 mmol) of tungstenocene dihydride was added by cannula over a 10 min period to a second 50 mL THF solution of 1.09 g (3.16 mmol) of diphenyltin dichloride and 4.409 mL (33.88 mmol) of collidine. During this addition the yellow tungstenocene solution turns a light orange color and a light-colored precipitate forms. This reaction mixture is stirred for a further 35 min, during which time additional precipitate forms. The solvent was then removed in vacuo, and the resulting orange solid was extracted with 200 mL of 1:1 hexanes/THF. After cannula filtration, solvent was removed in vacuo, producing a light orange solid. After two recrystallizations from THF/hexanes at −80 °C, 0.8184 g of analytically pure yellow-orange crystals (1.31 mmol, 42%) were recovered. ^{1}H NMR (THF-d_8): δ −12.65 (s, 1H, $J_{H^{119}Sn}$ = 175 Hz, J_{HW} = 71 Hz, W*H*), 4.74 (s, 10H, $J_{H^{119,117}Sn}$ = 10 Hz, Cp), 7.16 (t, 2H, *p*-Ph), 7.25 (t, 4H, *m*-Ph), 7.57 (d, 4H, $J_{H^{119,117}Sn}$ = 47 Hz, *o*-Ph). ^{13}C{^{1}H} NMR (THF-d_8): δ 149 ($J_{C^{119}Sn}$ = 250 Hz, J_{CW} = 11 Hz, Sn-*C*), 134 ($J_{C^{119,117}Sn}$ = 42 Hz, *o*-Ph), 126.0 (*m*-Ph), 125.9 (*p*-Ph), 73 (Cp). ^{119}Sn{^{1}H} NMR (THF-d_8): δ 119 ($J_{Sn^{183}W}$ = 1326 Hz). ^{183}W NMR (HMQC, THF-d_8): δ −3220. IR (KBr, cm^{-1}): ν (WH stretches) 1885, 1877 (m). IR (polyethylene, cm^{-1}): ν (SnCl stretch) 270 (s). MS (70 eV, EI): *m/z* 624 [M]$^+$, 588 [M − Cl]$^+$, 547 [M − Ph]$^+$, 470 [M − 2Ph]$^+$, 314 [Cp_2W]$^+$. Mp (sealed capillary): 190−195 °C. Anal. Calcd for $C_{22}H_{21}WSnCl$: C, 42.39; H, 3.40. Found: C, 42.52; H, 3.47.

Synthesis of Chlorobis(cyclopentadienyl)tungsten-di-*tert*-butyltin Chloride ($Cp_2WClSnCl^tBu_2$, 2a). A 20 mL flask with high-vacuum Teflon stopcock was charged with a 10 mL $CHCl_3$ solution containing 0.80 g of $Cp_2WHSnCl^tBu_2$ (1.53 mmol, **1a**). This solution was heated for 2 days at 50 °C, during which time the color changed from dark orange to wine red with no observable precipitate. The solution was then transferred to a 50 mL Schlenk flask, carefully layered with 30 mL of hexanes, and allowed to sit for 1 week. Over this diffusion period, many blocky crystals formed at the interface between the two solvent layers and the $CHCl_3$ layer lightened in color. Isolation of these black crystals yielded 0.622 g (1.01 mmol, 66%) of $Cp_2WClSnCl^tBu_2$ (**2a**) contaminated with a very small amount (>2%) of **1a**. A second recrystallization from $CHCl_3$/hexanes (∼1:6) produced 0.46 g (0.744 mmol, 49%) of analytically pure **2a**. ^{1}H NMR (THF-d_8): δ 1.33 (s, 9H, $J_{H^{119}Sn}$ = 62 Hz, ^{t}Bu), 5.21 (s, 10H, $J_{H^{119,117}Sn}$ = 6 Hz, Cp). ^{13}C{^{1}H} NMR (THF-d_8): δ 33 ($J_{C^{119}Sn}$ = 7 Hz, *C*H$_3$), 41 ($J_{C^{119}Sn}$ = 187 Hz, J_{CW} = 8 Hz, Sn*C*), 87 ($J_{C^{119}Sn}$ = 5 Hz, Cp). ^{119}Sn NMR (THF-d_8): δ 98 ($J_{Sn^{183}W}$ = 947 Hz). ^{183}W{^{1}H} NMR (THF-d_8): δ −1463. ^{1}H NMR ($CDCl_3$): δ 1.35 (s, 9H, $J_{H^{119}Sn}$ = 74 Hz, ^{t}Bu), 5.16 (s, 10H, $J_{H^{119,117}Sn}$ = 6 Hz, Cp). ^{13}C{^{1}H} NMR ($CDCl_3$): δ 33 ($J_{C^{119}Sn}$ = 6 Hz, *C*H$_3$), 41 ($J_{C^{119}Sn}$ = 196 Hz, J_{CW} = 7 Hz, Sn*C*), 85 ($J_{C^{119}Sn}$ = 6 Hz, Cp). ^{119}Sn NMR ($CDCl_3$): δ 114 ($J_{Sn^{183}W}$ = 882 Hz). Anal. Calcd for $C_{18}H_{28}WSnCl_2$: C, 34.99; H, 4.57. Found: C, 35.09; H, 4.46.

Synthesis of Chlorobis(cyclopentadienyl)tungsten-diphenyltin Chloride ($Cp_2WClSnClPh_2$, 2b). A 20 mL flask with high-vacuum Teflon stopcock was charged with a 10 mL $CHCl_3$ solution containing 0.88 g of $Cp_2WHSnClPh_2$ (1.34 mmol, **1b**). This solution was heated for 2 days at 50 °C, during which time the color changed from dark orange to wine red with concomitant formation of a large amount of precipitate. The solvent was removed in vacuo, and the resulting red solid was slowly recrystallized at RT from hot THF layered with hexanes. A second recrystallization yielded dark red crystals weighing 0.620 g (0.943 mmol, 70.4%) of analytically pure $Cp_2WClSnClPh_2$ (**2b**). ^{1}H NMR (THF-d_8): δ 5.15 (s, 10H, $J_{H^{119,117}Sn}$ = 7 Hz, Cp), 7.23 (m, 6H, *m,p*-Ph), 7.79 (d, 4H, $J_{H^{119,117}Sn}$ = 40 Hz, *o*-Ph). ^{13}C{^{1}H} NMR (THF-d_8): δ 147 ($J_{C^{119}Sn}$ = 288 Hz, J_{CW} = 8 Hz, Sn-*C*), 137 ($J_{C^{119,117}Sn}$ = 39 Hz, *o*-Ph), 129.0 (*p*-Ph), 128.8 (*m*-Ph), 88 (Cp). ^{119}Sn{^{1}H} NMR (THF-d_8): δ −133 ($J_{Sn^{183}W}$ = 1201 Hz). ^{183}W{^{1}H} NMR (THF-d_8): δ −1411. MS (70 eV, EI): *m/z* 658 [M]$^+$, 624 [M − Cl]$^+$, 586 [M − Ph/M − 2Cl]$^+$, 545 [M − PhCl]$^+$, 349 [M − $SnPh_2Cl$]$^+$, 314 [Cp_2W]$^+$, 78 [PhH]$^+$. Mp (sealed capillary): 274−276 °C. Anal. Calcd for $C_{22}H_{20}WSnCl_2$: C, 40.17; H, 3.06. Found: C, 40.32; H, 3.07.

Variable-Temperature NMR Study of 1a,b; 2a,b; and 4. THF-d_8 solutions of **1a**, **1b**, **2a**, **2b**, and **4** were prepared under argon atmosphere and introduced into 8 in. NMR tubes, which were then attached to a stopcock by way of a Cajon Ultratorr fitting and cooled to liquid nitrogen temperature. After the headspace above the frozen solution was evacuated, the tubes were sealed under reduced pressure and thawed at room temperature. ^{1}H and ^{119}Sn{^{1}H} NMR spectra were acquired at subambient temperature. The temperature inside the NMR probehead was monitored and regulated with a Bruker BVT-3200 temperature control unit equipped with a BTO-2000 thermocouple, using evaporated N_2 as coolant. The thermocouple had previously been calibrated against a 4% methanol in d_4-methanol standard.[33] Spectral data were referenced at room temperature as described above in the General Comments section, and the same spectral reference values (Bruker parameter SR) were utilized at all temperatures. Results are summarized in Figure 1.

X-ray Crystal Structure Determination of 1a,b; 2a,b; and 4. Crystals suitable for X-ray diffraction analysis were grown from THF/hexanes at −80 °C (**1a**,**b**, **4**), $CHCl_3$ at RT (**2a**), or CH_2Cl_2 at −80 °C (**2b**). Single crystals were cut to appropriate size under Paratone and mounted on a glass capillary on the goniometer head. Data were collected on a Nonius KappaCCD diffractometer at 190(2) K (cold N_2 gas stream), using Mo Kα graphite-monochromated radiation (λ = 0.71073 Å) with standard CCD data collection techniques. Lorentz and polarization corrections were applied to the data, and absorption corrections using the multiscan technique were utilized. The computer programs Denzo and Scalepack from the HKL software package were used for data reduction, and structure refinement was performed with the WinGX software package. The space groups were assigned on the basis of systematic absences in the observed reflections. The structures were initially solved using direct methods with SHELXS-97 and were refined by full-matrix least-squares techniques using SHELXL-97. All non-hydrogen atoms were refined with aniso-

(33) Geet, A. L. V. *Anal. Chem.* **1970**, *42*, 679−680.

tropic thermal parameters. In the case of **2b**, rigid bond restraints were used during the final stages of refinement for one of the cyclopentadienyl ligands due to the occurrence of unreasonable anisotropic thermal parameters for one of the ring carbons. The positions of hydrogen atoms located on carbon atoms were calculated using program defaults and subsequently refined using the riding model. The hydrides located on the tungsten in **1a**, **1b**, and **4** were found from a difference map near the end of the optimization and are located in chemically reasonable positions. Details of the crystals, data collections, and structure refinements are found in Table 2.

Acknowledgment. The authors thank Dale Swenson for acquisition of the X-ray diffraction data and useful discussions regarding the solution and refinement of complexes **1**, **2**, and **4**. The authors also thank Lou Messerle, Fred Hagemeister, and Kris McNeill for useful discussions. Funding for this research was supported in part by the American Chemical Society–Petroleum Research Fund (40520-GB3).

Supporting Information Available: Tables of positional and thermal parameters and bond distances and angles for **1**, **2**, and **4**. ORTEP diagrams and figures illustrating the calculated structure for **2**. Details of the computational studies of **1**–**4**. These materials are available free of charge on the Internet at http://pubs.acs.org.

OM049006D